Pergamon

PII: S0042-6989(96)00041-7

Vision Res., Vol. 36, No. 18, pp. 2849–2864, 1996

Printed in Great Britain
0042-6989/96 $15.00 + 0.00

Color Appearance of Mixture Gratings

KARL-HEINZ BÄUML,* BRIAN A. WANDELL†

Received 18 September 1995; in revised form 22 January 1996

We have examined how color appearance varies with spatial pattern. Subjects set color-matches between a uniform, 2 deg matching field and bars within squarewave patterns (1, 2 and 4 c/deg) or the superposition of these squarewaves. The matches were set using squarewaves and squarewave mixtures with many different colors and contrasts.

The color-matches satisfied the basic properties of a linear system to within a tolerance of twice the precision of repeated matches. Matches satisfied contrast-homogeneity: the contrast of the matching field was proportional to the contrast of the squarewave pattern or the mixture of squarewave patterns. Matches also satisfied pattern-superposition: if a bar in one squarewave matched one uniform field, and a bar in a second squarewave matched a second uniform field, the superposition of the two squarewave bars matched the superposition of the uniform matching fields.

Matches are predicted by a model in which the color at a location is predicted by the responses of three linear, pattern–color separable mechanisms. As the individual mechanisms are pattern–color separable, meaningful pattern and color-responsivity functions can be estimated for each of the mechanisms. The estimated color-responsivity functions, based only on asymmetric color-matches, have an opponent-colors organization. Copyright © 1996 Elsevier Science Ltd.

Appearance Colour Pattern Separability

INTRODUCTION

Color appearance depends on many different elements of the visual pathway, including the optical aberrations of the eye, light adaptation and the neural computations that interpret objects, light sources and distance relationships. In this and a related series of papers, we have analyzed how color appearance depends on some of these factors (Brainard & Wandell, 1992; Wandell, 1993, 1995; Poirson & Wandell, 1993, 1996; Marimont & Wandell, 1994; Bäuml, 1994, 1995; Chichilnisky & Wandell, 1995). Our work has been based on simple experimental images, viewed at moderate intensities on cathode ray tube (CRT) devices. Two principles have emerged.

First, we have studied how color appearance depends on the ambient illumination as established by the background color. The color appearance changes caused by changes in the background mainly can be explained by assuming that the signals from the three cone classes are scaled by a factor that depends on the background color. This classic notion, called von Kries adaptation, has had a long and controversial history. In our experimental measurements of color appearance on CRT display devices, simple variants of this model predict performance quite well (Walraven, 1976; Werner & Walraven, 1981; Brainard & Wandell, 1992; Fairchild & Lennie, 1992. Bäuml, 1995; Chichilnisky & Wandell, 1995), although there are some small and systematic deviations (Mausfeld & Niederee, 1993; Chichilnisky & Wandell, 1996). This general principle of receptor scaling has gained enough acceptance that it is being proposed as an important component in modern color appearance models that are being considered for international standards (e.g. Fairchild & Berns, 1993).

Second, we have studied how color appearance depends on spatial pattern. The color appearance of a spatial squarewave pattern depends on the spatial frequency of the squarewave. We have found that the change in color appearance with spatial frequency can be explained by assuming that signals from three opponent-colors mechanisms are scaled by a gain factor that depends on the local spatial frequency content of the image. This model is consistent with common engineering practice, in which it is well known that color appearance becomes progressively desaturated as the spatial frequency of the stimulus increases. We have captured this qualitative observation in laboratory measurements and modeled the phenomenon quantitatively (Poirson & Wandell, 1993, 1996).

Here, we report on new measurements of how color appearance depends on spatial pattern. Our initial measurements were based on simple squarewave stimuli.

*To whom all correspondence should be addressed at: Institut für Psychologie, Universität Regensburg, 93040 Regensburg, Germany [*Email* heinz@rpss3.psychologie.uni-regensburg.de].

†Department of Psychology, Stanford University, Stanford, CA 94305, U.S.A.

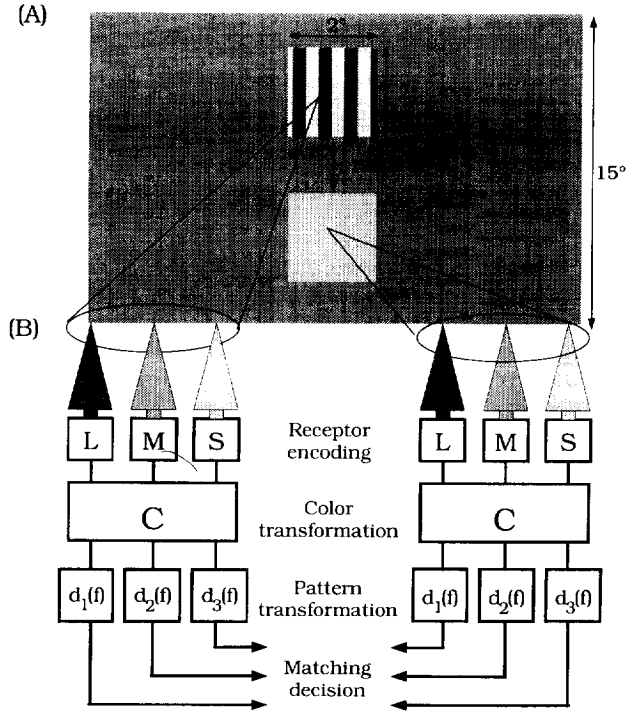

FIGURE 1. Pattern–color separable model. (A) Subjects set color appearance matches between a bar in the squarewave gratings and a uniform field. (B) In the first stage of the model, the mean rate of cone absorptions caused by the bar and the uniform matching box undergo a linear color transformation into an intermediate color representation. In the second stage, the intermediate color representation values are each scaled by an amount that depends on the local spatial pattern (f or f_o). The squarewave bar and the uniform box appear to match when the final, scaled representations are equal.

A general theory that explains the color appearance of more complex texture patterns must be able to predict the appearance of patterns formed by the sum of squarewaves from measurements of the appearance of the squarewaves in isolation. So, in this study, we made measurements of the appearance of squarewave gratings and their spatial mixtures. The squarewaves and their sums were presented on a uniform background field. They were shown in a common phase and orientation, but they were varied in color and contrast.

To measure the color appearance of our test patterns, subjects adjusted the appearance of a uniform matching box to match the appearance of different bars within the test patterns. We tested two empirical properties of these asymmetric color-matches. First, we tested whether the matches satisfied contrast-homogeneity. Suppose that a bar within a pattern formed by the mixture of squarewaves is matched by a uniform matching box. If we double the contrast of the test pattern, will the contrast of the matching box also double? We confirm Poirson and Wandell's (1993) observation that contrast-homogeneity holds for simple squarewaves; we extend their observations to show that homogeneity also holds for sums of low frequency squarewaves. Second, we tested whether the matches satisfied pattern-superposition. Suppose that one of the two bars comprising a squarewave is matched by a uniform matching box, and that a bar in a second squarewave is matched by a second uniform matching box. Now, form the sum of the squarewave gratings such that the two bars superimpose. Will subjects match the superposition of the bars by the superposition of the matching boxes? Again, for the low spatial frequency range we examined, we find that this superposition test holds reasonably well. These results indicate that, to a first approximation, the matches can be described using linear models.

Finally, we asked how well our subjects' matches can be predicted using a pattern–color separable model (Poirson & Wandell, 1993). The general principles of the experiment and the model are shown in Fig. 1. Subjects set color appearance matches between the bars in squarewave gratings and a uniform patch. The pattern–color separable model begins with a representation of the cone absorptions caused by the bar and the uniform matching box. In the first stage of the model, the mean rate of cone absorptions undergoes a linear color transformation into an intermediate color representation. In the second stage, the intermediate color representation values are scaled by an amount that depends on the local spatial pattern. The squarewave bar and the uniform box appear to match when the final, scaled representations are equal. Such a pattern–color separable model has two useful properties. First, it provides a good account of data collected using simple squarewave gratings. Second, the parameters of the color transformation and the parameters defining the pattern responsivity can be estimated from the data.

In this paper, we show that this same model also accounts for the measurements we have made using mixtures of squarewave gratings. The model parameters we estimate from the grating mixtures are quite similar to the model parameters Poirson and Wandell estimated using simple squarewave gratings.

METHOD

Experimental task

Two observers with normal color vision served as subjects. One subject (AF) was naive about the purpose of the experiment, the other subject (KHB) was one of the authors. The subjects viewed the screen from about 2 m.

Throughout the experiment, the monitor displayed a neutral, 15 deg uniform background. The test patterns were vertical squarewave gratings, or mixture gratings, subtending 2 deg, superimposed upon the uniform background [see Fig. 1(A)]. The matching box was presented below the test pattern, separated from it by 1.5 deg of visual angle. Subjects looked back and forth between the test pattern and matching box, adjusting the phosphor intensities to obtain an appearance match, i.e. to make the matching box have the same hue, saturation and brightness as the test stimulus. They continued to adjust the matching box until they were satisfied that they had obtained a complete appearance match.

TABLE 1. Cone contrasts of the color pairs in the three squarewaves employed in the experiment*

	Cone contrasts of squarewaves			
	L-cone	M-cone	S-cone	Appearance description
S-W 1	0.575	0.568	–0.780	Greenish-yellow
	–0.575	–0.568	0.780	Purple
S-W 2	0.187	0.076	0.010	Rose
	–0.187	–0.076	–0.010	Turquoise
S-W 3	0.600	0.815	0.942	Orange
	–0.600	–0.815	–0.942	Light blue

*Only the highest cone contrast values are given. Spatial pattern is a uniform, square, 2 deg field. S-W: squarewave.

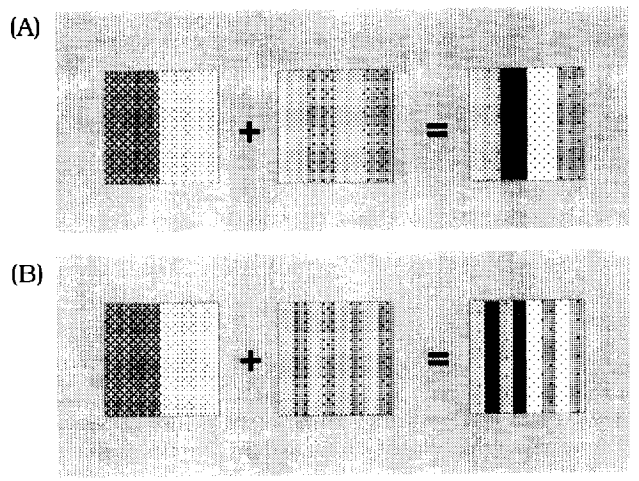

FIGURE 2. Mixture gratings. The mixture gratings consisted of sums of two squarewaves. The qualitative appearance of this type of pattern mixtures, using a light and dark shading, is shown for (A) the superposition of a 1 and 2 c/deg grating, and (B) the superposition of a 1 and 4 c/deg grating. Superposition was in sine-phase, and the patterns were all oriented vertically.

Color representation

The stimulus representation follows the one used by Poirson and Wandell (1993). The representation of the physical stimulus is based on the use of the Smith and Pokorny (1975) cone fundamentals. We use a version of the cone fundamentals that is normalized to a peak value of 1.0. The LMS coordinates of the uniform background are 5.322, 5.007 and 4.485. These three values are proportional to the rate of the photopigment absorptions created by a uniform field in the three cone classes for a standard observer. The CIE 1931 luminance and chromaticity coordinates of the background were $Y = 36.2$ cd/m^2, $x = 0.27$, $y = 0.30$.

We represent the matching box and the gratings as a cone-contrast modulation with respect to the uniform background, $s = (\Delta L/L, \Delta M/M, \Delta S/S)$. We define the color direction of a stimulus to be the unit length vector:

$$\frac{1}{||s||}\mathbf{s},$$

where $||s||$ is the vector length of the cone-contrast vector, **s**.

Pattern representation

Subjects made matches to isolated squarewaves and to mixture gratings that consisted of sums of squarewaves. Specifically, they set matches to the two differently colored bars of a squarewave grating, and the four differently colored bars of a mixture grating.

We constructed isolated squarewave gratings of 1, 2 and 4 c/deg. The squarewaves were created in one of three color directions. The complementary bars in the grating appeared greenish yellow/purple, turquoise/rose, or orange/light blue. The color directions of these squarewave patterns are shown in Table 1.

The mixture gratings consisted of sums of two squarewaves. The qualitative appearance of this type of pattern mixtures, shown using only light and dark shading, is shown in Fig. 2. The patterns were all oriented vertically, and superposition was in sine-phase. Asymmetric matches were obtained using grating sums formed by component squarewaves with different color directions and also by components with the same color direction. A variety of contrast levels was used for each of the components. The same three color directions were used for the squarewave components whether we measured in isolation or as part of a grating mixture.

The mixture contrasts of the gratings were varied in two different ways. In one method, the ratio of cone contrasts of a mixture grating's two squarewaves was fixed, and the cone contrasts of the squarewaves were varied at four different levels. Three different contrast ratios were used (3:1, 1:1 and 1:3). Measuring color appearance for these test patterns provided a test of contrast-homogeneity for mixture gratings.

In the second method, the cone contrast of the mixture grating's 2 or 4 c/deg squarewave was fixed, and the cone contrast of the mixture grating's 1 c/deg squarewave was varied at four different contrast levels. The contrast of the 2 or 4 c/deg squarewave was fixed at four different contrast levels. Measuring color appearance for these test patterns provided a test of pattern-superposition.

Subject AF made adjustments to mixture gratings consisting of sums of a 1 and a 2 c/deg squarewave. In addition, he made matches to isolated squarewaves of 1 and 2 c/deg. Subject KHB made adjustments to mixture gratings consisting of sums of a 1 and a 2 c/deg squarewave, as well as of a 1 and a 4 c/deg squarewave. In addition, he made matches to isolated squarewaves of 1, 2 and 4 c/deg. Our two subjects' data include about 380 different spatial frequency and color conditions, with two matches in each condition. Table 2 provides a more detailed description of the experimental conditions for the two subjects.

Equipment and monitor calibration

We presented our stimuli on a 60 Hz non-interlaced color monitor (Hitachi, model 4319) controlled by a graphics card (TrueVision, model ATVista) in an IBM PC-AT. We measured the spectral emission of the

TABLE 2. Squarewaves and mixture gratings employed in the experiment*

Experimental gratings			
First component	Second component	Contrast combinations	Subject
S-W 1, 1 c/deg	—	4	AF, KHB
S-W 1, 2 c/deg	—	4	AF, KHB
S-W 1, 4 c/deg	—	4	KHB
S-W 2, 2 c/deg	—	4	AF, KHB
S-W 3, 1 c/deg	—	4	AF
S-W 3, 2 c/deg	—	4	AF
S-W 1, 1 c/deg	S-W 1, 2 c/deg	28	AF, KHB
S-W 1, 1 c/deg	S-W 1, 4 c/deg	28	KHB
S-W 1, 1 c/deg	S-W 2, 2 c/deg	28	AF, KHB
S-W 3, 1 c/deg	S-W 3, 2 c/deg	28	AF

*The gratings were isolated squarewaves and mixture gratings consisting of sums of squarewaves. S-W: squarewave. For each squarewave, one contrast combination means two asymmetric color matches. For each mixture grating one contrast combination means four asymmetric color matches.

monitor phosphors using a PhotoResearch PR-703A Spectral Scanner, and the digital control value to phosphor intensity relation (gamma curve) using a PhotoResearch 2009 Tele-Photometer. We tested for monitor phosphor additivity, verifying it to good approximation (Brainard, 1989; Wandell, 1995's Appendix B). All these measurements were taken weekly. Additionally, periodic stability checks were done with a hand-held Minolta ChromaMeter.

In this experiment, test pattern and matching box were presented at different locations on the screen. To compensate for local variations in the emission of the monitor's phosphors and the gamma curves, all the above measurements were done separately for the screen locations where test pattern and matching box were presented. Phosphor spectra and gamma curves measured at the center of the test pattern, or matching box, were used to control our stimuli.

Model evaluations

We report tests of several models of the asymmetric matching data. Each model contains several transformations that represent the free parameters of the model. To choose the best parameters for each model, we minimized the difference between theoretically predicted and empirically observed matches using an error term that is normalized by the estimated covariance matrix of the match settings.

As we have only two replications, we cannot use the match covariance for individual data points. Instead, we normalize the observed difference between prediction and observation using the global covariance matrix, Δ, derived by combining all of the subject's matches. Suppose the column vector, $\mathbf{e}_i$, denotes the difference between the predicted and observed cone contrasts. Then, we estimate the model parameters subject to minimization of the quantity:

$$\frac{1}{n}\sum_{i=1}^{n}(\mathbf{e}_i^t\Delta^{-1}\mathbf{e}_i)^{1/2}.$$

Intuitively, this error measure is equivalent to (a) transforming the model deviations in a new coordinate frame where the distribution of errors are independent and have unit variance; and (b) using the Euclidean distance in that coordinate frame as the error measure. This approach to model fitting was used by Poirson and Wandell (1993) and Bäuml (1994, 1995). Poirson and Wandell showed that the error measure yields the same model fit, independent of the original coordinate frame (up to a linear transformation) that is used to represent the data.

RESULTS

The presentation of the results is organized into three sections. First we review the precision of the asymmetric color-matching task by comparing the repeated matches made by observers. The precision of repeated matches is important because we use the covariance matrix derived from these matches to measure the size of the pattern effects on color and to evaluate the precision of the model fits to the data.

The empirical properties of contrast-homogeneity and pattern-superposition are reviewed in the second and third sections. All linear models of the asymmetric matches imply that these two general properties should hold. Hence, we evaluate these properties prior to considering specific linear models in the next section.

Precision of repeated matches

Figure 3 provides a visual representation of the precision of repeated matches. The three panels of the figure show the cone contrast of the mean match on the vertical axis and the cone contrast of the individual matches on the horizontal axis; each panel represents data for one of the three cone types. The deviation about the solid diagonal line is a visual representation of the match precision.

Figure 3 is an incomplete representation of the full covariance matrix of match errors; only the within-cone type predictions are shown. Even so, from this partial representation it is clear that the variance of the matches

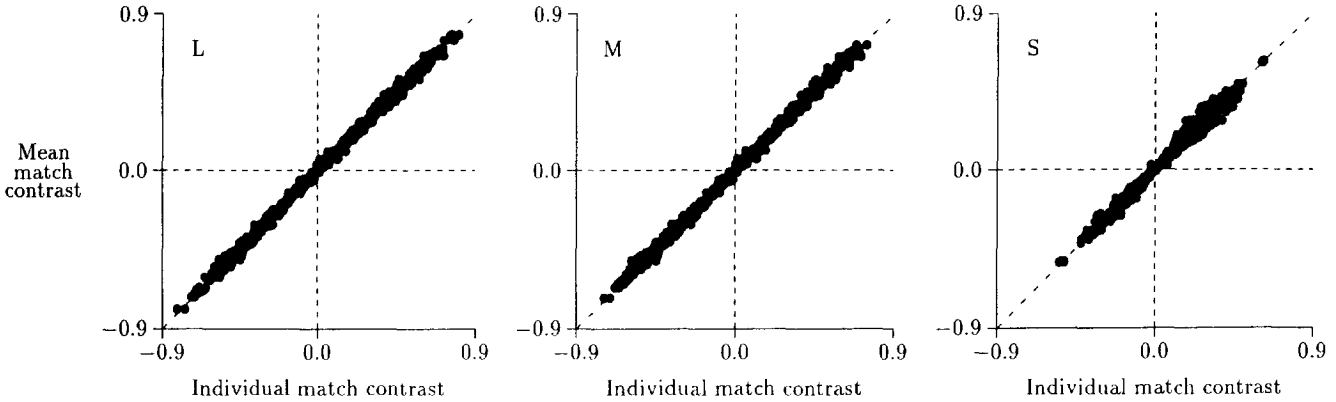

FIGURE 3. Visual representation of the precision of the measurements. Cone contrast of mean match on the vertical axis is plotted against cone contrast of the individual matches on the horizontal axis. Each panel refers to either the L, M or S cone type. The origin of the graph represents the mean background (subject KHB).

for the S cones is larger than the variance of match settings for the other two cone classes.

As we describe in the Method section, we evaluate model errors relative to the covariance of repeated matches. To the extent that the errors are normally distributed, we expect roughly 50% of the data to have a normalized error of less than about 1.5.

The effect of spatial pattern

We can estimate the size of the effect of spatial pattern on the color appearance gratings as follows. Were there no effect of pattern, the match and pattern contrast would be the same. Hence, differences between these two values measure the effect of pattern on color appearance. For subject KHB, the average difference between the match and a pattern involving a 4 c/deg grating (the highest used by this subject) was 11.47; about one-fifth of the matches differed from the bar stimulus by 18.2 units or more. For the same subject, the average difference between the match and a pattern involving a 2 c/deg grating was 10.91; about one-fifth of the matches differed from the bar stimulus by 18.0 units or more. For subject AF, the average error for all matches involving a 2 c/deg grating (the highest used by this subject) was 5.39; about one-fifth of the matches differed from the bar stimulus by 8.5 units or more. Hence, even for 2 c/deg patterns, pattern has a significant effect on color appearance; at 4 c/deg the effects are quite substantial.

In these and other asymmetric color-matching experiments using patterns, we have found that many subjects find it quite difficult to set color-matches to fine patterns. We have never had a subject who had difficulties at 2 c/deg, but AF struggled with 4 c/deg patterns and all of our subjects found setting such matches at 8 c/deg or higher either very difficult or impossible. Why this should be is an interesting question in itself, because subjects have no difficulty seeing the bars, they simply have difficulty in identifying the color of the bars. The appearance is variable and hard to describe compared to the stability of wide targets.

Contrast-homogeneity and pattern-superposition

A main goal of the present study is to evaluate how well asymmetric color-matches to individual gratings can be used to predict asymmetric color-matches to grating mixtures. To evaluate the ability to generalize from individual gratings to grating mixtures, we will test a collection of linear models. Hence, our presentation of

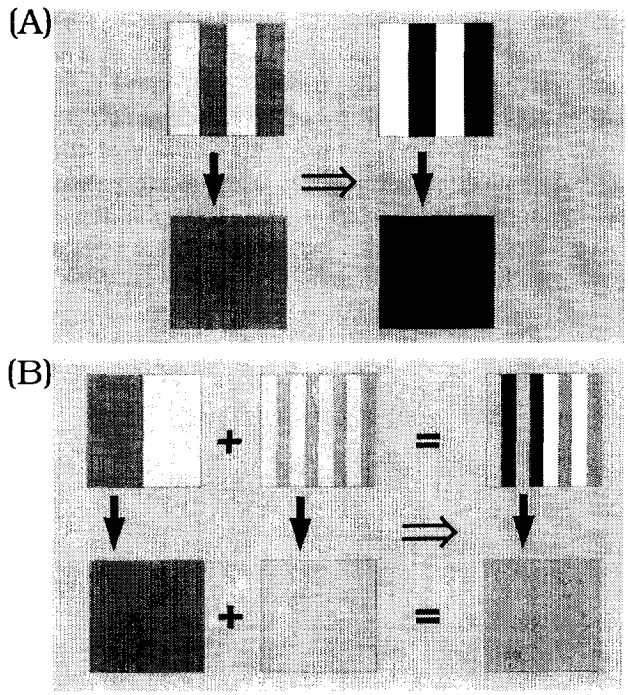

FIGURE 4. Tests of contrast-homogeneity and pattern-superposition are shown in graphical form. (A) Suppose that a bar within a squarewave pattern is matched by a uniform matching box. Will doubling the contrast of the test pattern also double the contrast of the matching box (contrast-homogeneity)? (B) Suppose that one of the two bars comprising a squarewave is matched by a uniform matching box, and that a bar in a second squarewave is matched by a second uniform matching box. Will the superposition of these bars be matched by the superposition of the uniform matching fields (pattern-superposition)?

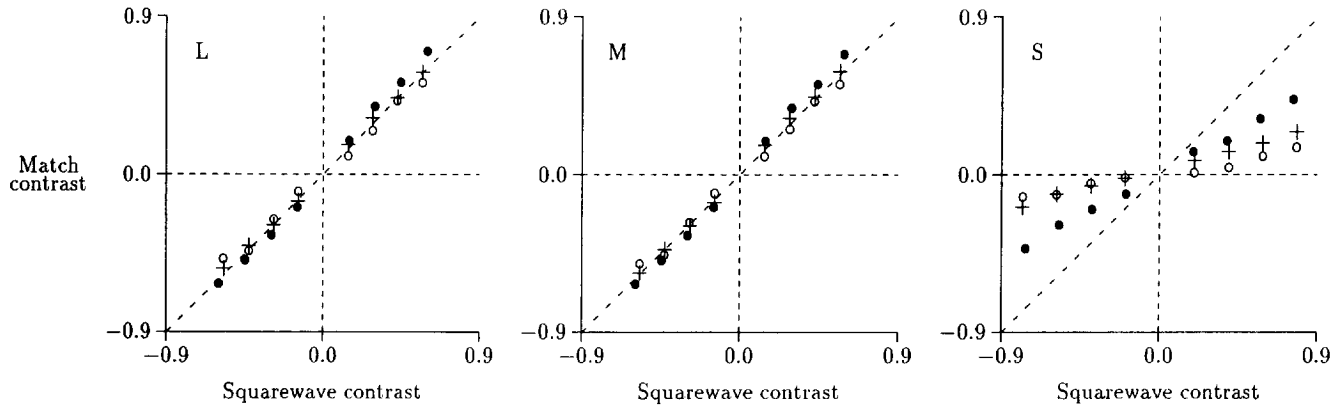

FIGURE 5. Tests of contrast-homogeneity for isolated squarewave gratings. Full color-matches to squarewaves of varying contrast and varying spatial frequency (1, 2 and 4 c/deg) are shown. The squarewaves' color direction was greenish-yellow/purple. The horizontal axis of each panel is the cone contrast of the squarewaves' bars, the vertical axis is the cone contrast of the matching box. The three panels refer to the three different cone types (● = 1 c/deg, + = 2 c/deg, ○ = 4 c/deg; subject KHB).

the data begins with a description of empirical measurements of the two basic properties of linear models: contrast-homogeneity and pattern-superposition.

Contrast-homogeneity can be tested as follows [see Fig. 4(A)]. Suppose that the observer matches a bar in a pattern whose components are (t_i) by a uniform box with contrast m. Now, suppose we scale the contrasts of all of the squarewave components so that the new pattern contrasts are at_i. Contrast-homogeneity holds if the observer matches the bar in the new pattern with a box of contrast am.

Pattern-superposition can be tested as follows [see Fig. 4(B)]. Suppose the observer matches a bar in a single squarewave pattern, whose contrast is t_1, with a matching box of contrast m_1, and a bar in a second squarewave pattern with contrast t_2 with a matching box of contrast m_2. Now, superimpose the two squarewave patterns so that the matched bars overlap. We expect that the match to the superposition of the bars will be the superposition of the matches, i.e. the match to the pattern (t_1, t_2) will be $m_1 + m_2$.

When both contrast-homogeneity and pattern-superposition hold, it is possible to describe the matching process using linear models. Deviations from these two properties will limit how well any linear model-relating pattern and match cone contrasts, measured prior to chromatic aberration can fit the data.

Contrast-homogeneity. Figure 5 shows some typical data on how subjects' matches to isolated squarewaves varied with cone contrast and spatial frequency of the gratings. The three panels refer to the three different cone types. The horizontal axis of each panel is the cone contrast of the squarewave, the vertical axis is the cone contrast of the matching box. The panel origin represents the mean background.

Figure 5 shows matches to patterns at 1, 2 and 4 c/deg for squarewaves in the greenish-yellow/purple color direction. For each spatial frequency, matches were made to both bars at four contrast levels. Each data point represents the average of two matches to a single bar.

For all three spatial frequencies and all three cone types, the match contrast scales linearly with the spatial

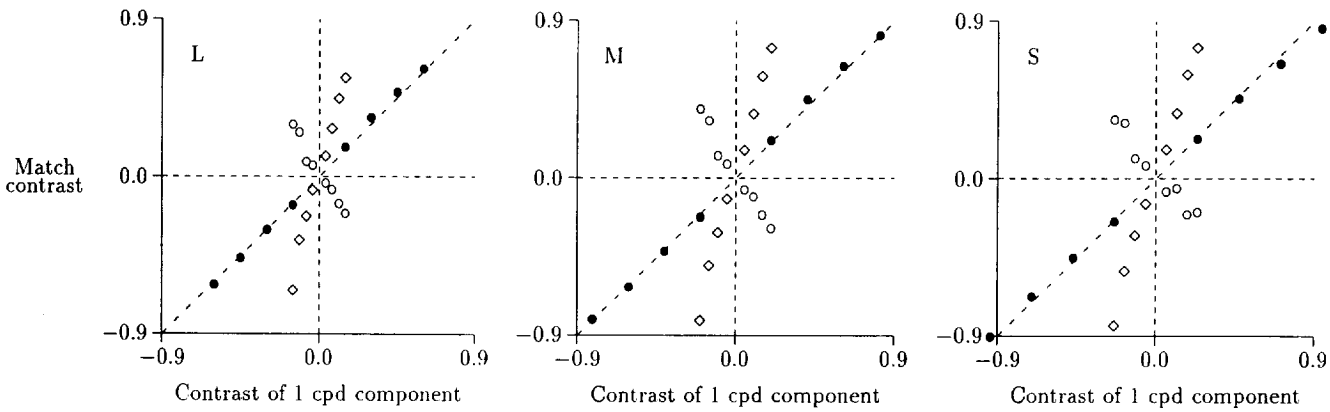

FIGURE 6. Tests of contrast-homogeneity for mixture gratings. Full color-matches to mixture gratings consisting of a 1 and a 2 c/deg squarewave are shown. The color direction of both squarewaves was orange/light blue. The contrast of the mixture grating was varied, but the contrast ratio of the two components was held fixed (1:3). The horizontal axis of each panel is the cone contrast of the 1 c/deg squarewave, the vertical axis is the cone contrast of the matching box. The three panels refer to the three different colic types (◇, ○ match to mixture grating, ● matches to isolated squarewave of 1 c/deg; subject AF).

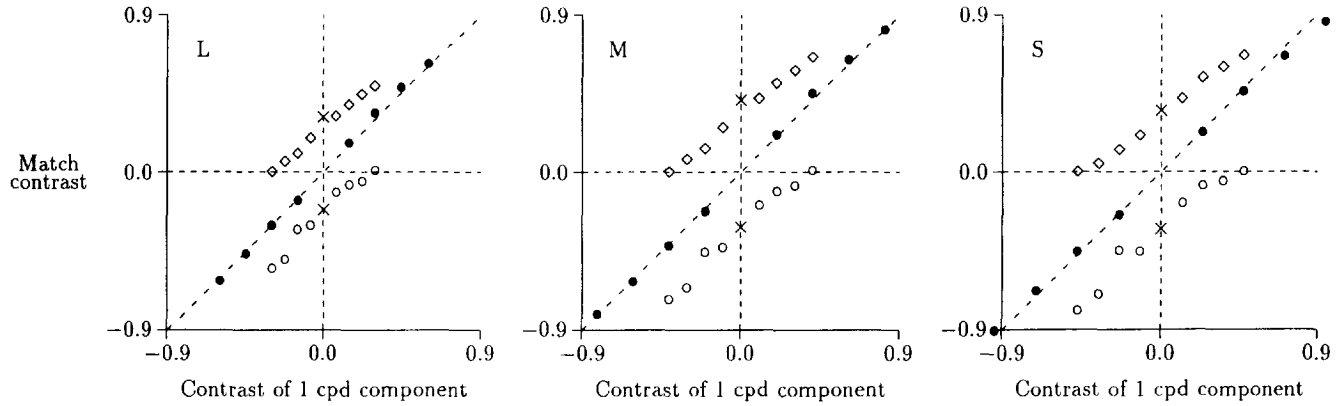

FIGURE 7. Tests of pattern-superposition for mixture gratings. Full color-matches to mixture gratings consisting of a 1 and a 2 c/deg squarewave are shown. The two squarewaves had the same color direction as those in Fig. 6. The contrast of the mixture gratings was varied by fixing the contrast of the 2 c/deg squarewave and varying the contrast of the 1 c/deg squarewave. The axes are identical to those in Fig. 6 (◇, ○ match to mixture grating, ● matches to isolated 1 c/deg squarewave, × matches to isolated 2 c/deg squarewave; subject AF).

pattern contrast, consistent with contrast-homogeneity. To the extent that the measurements for each of the three frequency conditions deviate from a line of unit slope, the matches show an effect of pattern on color appearance. With increasing spatial frequency, the matches tend to deviate from physical matches. This effect is most clearcut for the S cone data.

Figure 6 shows results from matches to a 1 c/deg grating (solid symbols) and to the bars in a mixture grating formed by superimposing 1 and 2 c/deg squarewaves (open symbols). The ratio of the cone contrast of the squarewaves in the mixture was fixed at 1:3. The contrast of the mixture was varied by scaling the contrast of the components equally. Both of the squarewaves had an orange/light blue color direction. For all of the data points, the horizontal axis of each panel represents the cone contrast of the 1 c/deg component, and the vertical axis is the cone contrast of the matching box. The panel origin represents the mean background.

Again, for each bar and each cone type, the data fall along straight lines. Thus, the data are consistent with the predictions of contrast-homogeneity. Notice that the negative slopes result from the superposition of dark bars of 2 c/deg patterns on bright bars of 1 c/deg patterns, and from the superposition of bright bars of 2 c/deg patterns on dark bars of 1 c/deg patterns.

Pattern-superposition. Figure 7 shows the results of a test of pattern-superposition. The figure shows matches to grating mixtures in which the cone contrast of one squarewave component was fixed and the cone contrast of the second component was varied. The spatial frequencies and color direction of the squarewave components were the same as those used for the data of Fig. 6. The contrast of the 1 c/deg component was varied at four different contrast levels; the contrast of the 2 c/deg component was fixed.

If pattern-superposition holds, then the matches to this set of mixtures must fall on two lines that are parallel to the 1 c/deg appearance line. The vertical distance of these lines from the 1 c/deg appearance line must be equal to the contrast matched to the isolated 2 c/deg squarewave component. To a first approximation, the data are consistent with the prediction of pattern-superposition.

Figure 8 shows a larger set of tests of contrast-homogeneity and pattern-superposition. In each panel of the figure, the horizontal axes measure the cone contrast of the two grating mixture components. The vertical axis measures the contrast of the matching box. The data in these figures include: matches for which the cone contrast of the components is varied equally, holding the ratio of the components' cone contrast fixed; matches to mixture gratings where only the cone contrast of one component is varied; and matches to isolated squarewaves. The squarewaves were 1 and 2 c/deg, appearing greenish yellow/purple and turquoise/rose in isolation (A); and 1 and 4 c/deg, appearing both yellowish green/purple in isolation (B). About 250 data points are shown for each frequency combination and each cone type.

In each case, the viewing angle has been adjusted to make it evident that the matches from all of these conditions fall within a plane; i.e. the viewing angle is chosen to align with the plane so that we see only the thin edge of the plane in each panel. Viewed from other perspectives, the data spread out quite broadly across the space. As we show later, contrast-homogeneity and pattern-superposition predict that the data from all of these conditions should fall on a plane through the origin. Qualitatively, then, the fact that the data from all of these different conditions fall near a plane suggests that the linear models of the asymmetric color-matches are worth exploring.

MODELS

In this section, we use our measurements to evaluate several different ideas concerning pattern and color appearance. We begin by testing a pattern-dependent

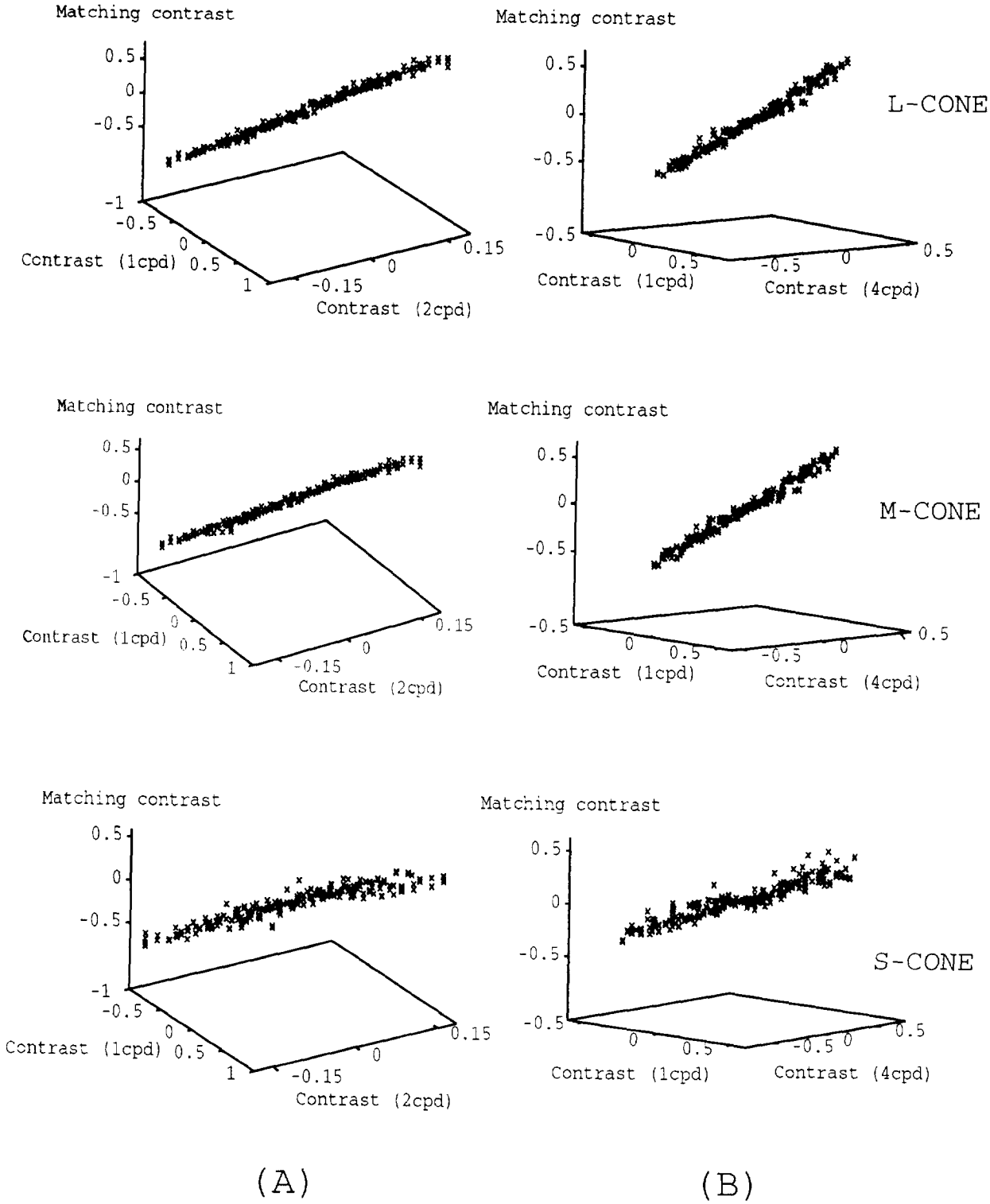

FIGURE 8. Tests of linearity of asymmetric color-matches. Full color-matches to mixture gratings are shown. Matching box contrasts are plotted as a function of the contrasts of the squarewave components. The data of a variety of contrast combinations are plotted, including matches to mixture gratings where the contrast ratio of the components is fixed and the contrast of both components is varied, matches to mixture gratings where only the contrast of one component is varied, and matches to isolated squarewaves. (A) A 1 c/deg squarewave appearing greenish yellow/purple and a 2 c/deg squarewave appearing turquoise/rose (subject AF). (B) A 1 and a 4 c/deg squarewave both appearing greenish yellow/purple (subject KHB). The three panels refer to the three different cone types. The view has been adjusted to emphasize the planarity of the settings.

linear model. This model tests the two main linearity assumptions of contrast-homogeneity and pattern-superposition. According to this model, each spatial pattern is transformed to a new color coordinate frame. The color coordinate frame for each pattern is free to depend upon the pattern. The matches to mixtures are predicted by the sum of these pattern-dependent representations.

Next, we evaluate a pattern–color separable linear

model. In this model, every stimulus is converted to the same three-dimensional color coordinate frame, independent of its spatial pattern. Then, each of the three dimensions of the color coordinate frame is scaled by a factor that depends on the spatial pattern of the test. Because the color coordinate frame does not depend on pattern, and the pattern-sensitive scaling does not depend on the stimulus color, this model captures the main idea of pattern–color separability. The pattern-dependent model and the pattern–color separable model represent the two main ideas of this paper, namely that the asymmetric color-matches of these low frequency targets can be described by a fundamentally linear model and that the individual mechanisms mediating color appearance, though not the observer as a whole, are separable with respect to pattern and color.*

Finally, we considered three variants of these models. The separable Minkowski model handles pattern and color separably, but combines the responses from different components of the mixture pattern by a nonlinear Minkowski pooling formula rather than a simple addition. The increment/decrement model was designed to evaluate whether the matches could be better predicted by fitting incremental and decremental cone absorptions (relative to the background) separately. The incomplete discounting model compares the match predictions when we add a constant term into the test pattern color representation.

Pattern-dependent linear model

The experimental measurements were designed to test two key aspects of linearity: contrast-homogeneity and pattern-superposition. When these two empirical properties hold, we can create a simple linear model of the contrast matches. The model relates the matching box contrasts to the test pattern contrasts through a linear equation that we call the pattern-dependent linear model.

Consider a mixture grating consisting of the sum of two squarewaves with frequencies f_1 and f_2. Suppose the cone contrasts of the component gratings are represented by the cone contrast vectors $\mathbf{s}_1$ and $\mathbf{s}_2$, so that the four possible bars are $\pm\mathbf{s}_1$, $\pm\mathbf{s}_2$. In the pattern-dependent linear model, we assume that there are two pattern-dependent matrices $\mathbf{T}_{f_1}$ and $\mathbf{T}_{f_2}$, each of which is 3×3. The matching cone contrast, m_s, to each of the four differently colored bars $\mathbf{s} = \pm\mathbf{s}_1 \pm \mathbf{s}_2$ of the mixture grating is predicted to be:

$$m_s = \pm\mathbf{T}_{f_1}\mathbf{s}_1 \pm \mathbf{T}_{f_2}\mathbf{s}_2.$$

The free parameters in this model are the nine entries of the transformations $\mathbf{T}_f$. Subject KHB made matches using three different squarewaves spatial frequencies so, to fit his 760 data points, the model includes 27 (3×9) parameters. Subject AF made matches with two different spatial frequencies so, to fit his 760 data points, the model includes 18 (2×9) parameters.

The observed and predicted cone contrasts using the pattern-dependent linear model for all of the asymmetric matches of one subject are shown in Fig. 9(A). This figure provides a visual representation of the overall quality of fit of the model which may be compared to the precision of repeated matches (Fig. 3). Relative to the estimated covariance matrix, the average error for this model is 3.42 for subject KHB and 3.08 for subject AF. If the data fit the model perfectly and all the deviations were explained by the precision of repeated matches, the average error would be 1.42 for subject KHB and 1.41 for subject AF. Hence, linearity captures the main effects to within a tolerance of twice the precision of repeated matches. As we discuss later, there may be some small systematic deviations.

Pattern–color separable model

The pattern-dependent model allows a separate color representation for each different pattern. This type of neural representation might arise, say, if the visual representation coded patterns into different spatial frequency bands and the color representations within these different bands were not well coordinated.

Alternatively, it is possible that, prior to segmentation based on pattern, the visual system transforms the entire spatial representation into a new color coordinate frame and that information within the different spatial frequency bands is formed from data in this one color coordinate frame. In this case, the representation of pattern and color information for each mechanism could be described as separable. This is the idea that we examine here.

The pattern–color separable linear model specializes the pattern-dependent linear model by adding the assumption that there is a single 3×3 linear transformation, $\mathbf{C}$, that is applied to the encoded image. This matrix maps the vector of color contrasts, $\mathbf{s}$, into a new color coordinate frame and the matrix is independent of the spatial pattern of the grating components. Pattern responsivity depends on a separate factor that scales each of the color coordinates. We can represent the three pattern-responsivity factors that scale the three color coordinates using a diagonal matrix, $\mathbf{D}_f$. Because only the diagonal matrix $\mathbf{D}_f$ depends on spatial pattern, but the matrix $\mathbf{C}$ does not, this model is a special case of the pattern-dependent linear model.

Analogous to the pattern-dependent linear model, we can express the relationship between the vector of test pattern cone contrasts and the vector of match cone contrasts using a matrix equation. Again, suppose the test pattern consists of the mixture of one squarewave with frequency f_1 and cone contrasts $\mathbf{s}_1$, and a second squarewave with frequency f_2 and cone contrasts $\mathbf{s}_2$. The relationship between the test contrasts and the match

*Retinal ganglion cell receptive fields are an example of a system that is not pattern–color separable, even though it is made from pattern–color separable component mechanisms. Specifically, the receptive fields commonly are modeled as the difference of signals from a pattern–color separable center and surround mechanisms. Because the spatio-temporal sensitivities of the center and surround differ, the receptive field of the retinal ganglion cell as a whole is not pattern–color separable.

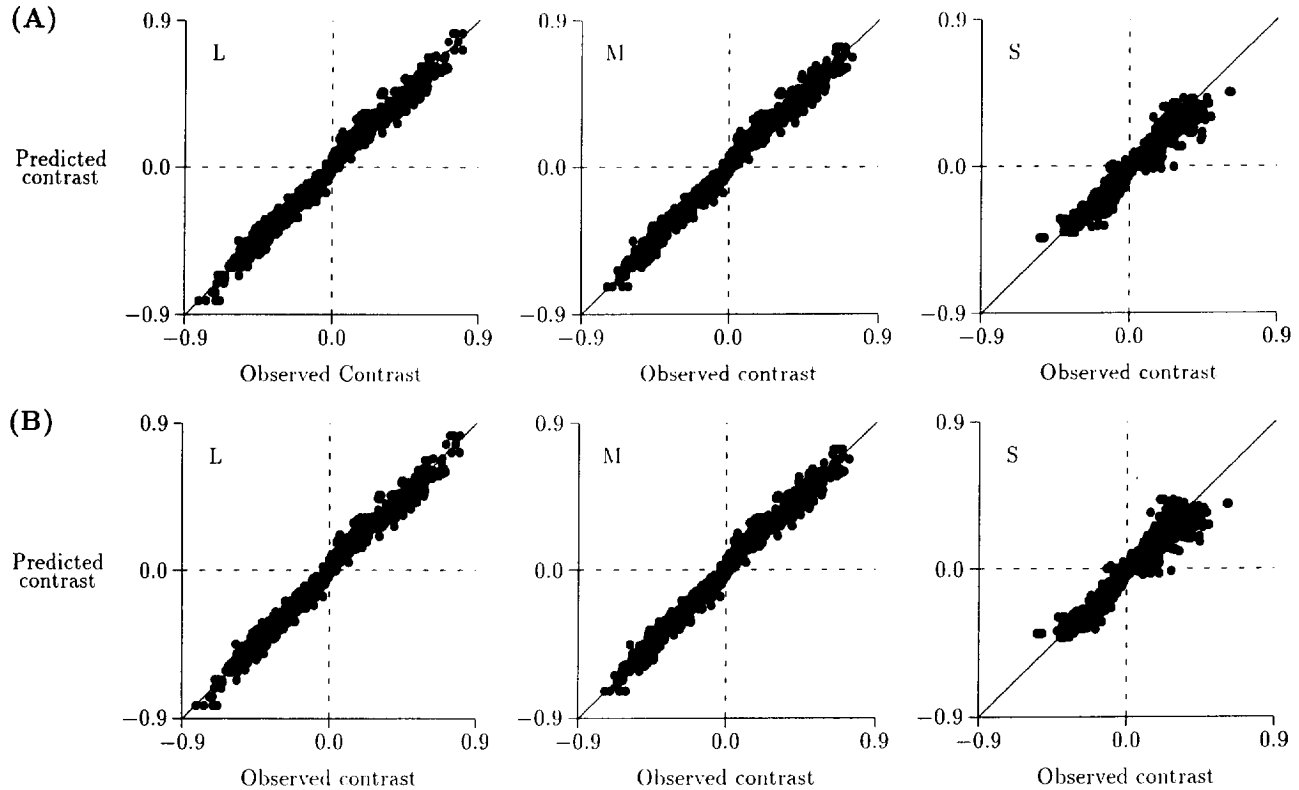

FIGURE 9. Quality of fit of two linear models. The observed vs predicted matches are shown using (A) the pattern-dependent linear model; and (B) the pattern–color separable model. Were the models perfect, all data points would fall on the diagonal line. The three graphs of each panel refer to the three different cone types and may be compared to the precision of repeated matches (subject KHB).

cone contrast vector, $\mathbf{m}_s$, for the four differently colored bars $\mathbf{s} = \pm\mathbf{s}_1 \pm \mathbf{s}_2$ is predicted to be:

$$\mathbf{m}_s = \mathbf{C}^{-1}[\pm\mathbf{D}_{f_1}\mathbf{C}\mathbf{s}_1 \pm \mathbf{D}_{f_2}\mathbf{C}\mathbf{s}_2].$$

This equation clarifies the relationship between the pattern-dependent linear model and the pattern–color separable linear model: in the pattern–color separable model, the general matrix $\mathbf{T}_f$ is replaced by the special matrix $\mathbf{C}^{-1}\mathbf{D}_f\mathbf{C}$.

We fitted the pattern–color separable model to the data of both subjects. For subject KHB, the model includes nine parameters for the matrix **C** and three parameters for each of the three spatial frequencies for a total of 18 ($3 \times 3 + 9$) parameters to describe the 760 data points. For subject AF, the model includes 15 ($2 \times 3 + 9$) parameters to describe the 760 data points.

Figure 9(B) shows the observed and predicted cone-contrasts using the pattern–color separable linear model for all of the asymmetric matches of subject KHB. The quality of the fit is similar to that observed using the pattern-dependent linear model [see Fig. 9(A)]. This also is confirmed quantitatively because the residual error for the separable model for subject KHB was 3.57 compared to 3.42 for the pattern-dependent model; for subject AF, the residual error was 3.09 compared to 3.08.

Several variants of the models

The basic linear models capture a good deal about performance under these conditions. We consider the important restrictions on our conditions to include the moderate luminance levels of display screens and the modest spatial frequency range we have used in these experiments. We shall return to discuss each of these limitations more fully later.

Even within this restricted experimental range, the model fits to the data are not perfect. We have examined several simple alternative models, but none of them has significantly improved the fit to the data.

First, we evaluated whether generalizing the rule of combination from simple addition to a Minkowski combination could improve the predicted matches. In this generalization, the vector of match cone contrasts is predicted to be related to the vector of stimulus cone contrasts by the rule:

$$\mathbf{m}_s = \mathbf{C}^{-1}[\pm\mathbf{D}_{f_1}\mathbf{C}\mathbf{s}_1 \otimes \pm\mathbf{D}_{f_2}\mathbf{C}\mathbf{s}_2],$$

where $\mathbf{m}_s$, $\mathbf{s}_1$ and $\mathbf{s}_2$ represent three-dimensional cone contrast vectors, and:

$$\mathbf{r} \otimes \mathbf{s} = (\mathbf{r}_i^{p_i} + \mathbf{s}_i^{p_i})^{1/p_i}$$

for $i = 1, 2, 3$. This rule includes the additive combination rule as a special case. In fact, the additive combination

TABLE 3. Color matrices C for the best-fitting pattern–color separable linear model*

Subject	Function	Color matrices C L cone	M cone	S cone
AF	B/W	0.697	0.331	–0.195
	R/G	2.000	–1.895	0.043
	Y/B	0.773	–1.271	1.037
KHB	B/W	0.783	0.240	0.067
	R/G	2.235	–2.588	0.363
	Y/B	0.038	–0.415	1.019

*Each row lists the cone weights used to construct the spectral responsivity functions shown in Fig. 10. The L, M and S cones are the Smith–Pokorny cone fundamentals, each normalized to a peak value of 1.0. B/W: black/white, R/G: red/green, Y/B: yellow/blue.

rule imposes the restriction $p = 1$ to hold simultaneously for all three mechanisms.

This model is less restrictive than the pattern–color separable linear model. It allows for three additional parameters to account for the weighting of the three mechanisms' responses. For subject KHB, the model therefore includes $21(3 \times 3 + 9 + 3)$ parameters to describe the 760 data points; for subject AF, it includes 18 $(2 \times 3 + 9 + 3)$ parameters.

This generalization, however, did not improve error substantially. For subject KHB, we found a residual error of 3.32 compared to 3.57 for the pattern–color separable linear model, for subject AF we found 3.08 compared to 3.09 for the pattern–color separable linear model.

Second, we evaluated the possibility that matches made to increments and decrements must be modeled by separate mechanisms. In several recent studies, mainly involving light adaptation, it has been suggested that the positive and negative stimulus contrasts are coded in separate ON and OFF pathways of the visual system with different color responsivities (Walraven, 1977; Krauskopf, 1980; White *et al.*, 1980; Schiller *et al.*, 1986; Whittle, 1986; Bowen *et al.*, 1989; du Buf, 1992; Mausfeld & Niederee, 1993; Chichilnisky & Wandell, 1996). According to these models, the signals from the incremental and decremental pathways are subject to different adaptation and are then recombined into the responses of three parallel neural mechanisms.

To evaluate whether the residual error could be reduced using this idea, we evaluated a generalization of the pattern–color separable model. In this generalization, the columns of the color transformation matrix **C** were allowed to vary depending on the sign of the stimulus contrast. This generalization results in nine additional parameters because there is one set of columns (nine parameters) for the positive cone contrasts and a second set of columns (nine parameters) for the negative cone contrasts. For subject KHB, the model therefore includes 27 $(3 \times 3 + 18)$ parameters to describe the 760 data points; for subject AF, it includes 24 $(2 \times 3 + 18)$ parameters.

Generalizing the pattern–color separable model to separately encode increments and decrements did not substantially improve the fit to the data. For subject KHB, we found a residual error of 3.32 compared to 3.57 for the pattern–color separable model; for subject AF, we found a residual error of 2.91 compared to 3.09 for the pattern–color separable linear model.

A third idea that we evaluated was the question of whether we might predict the matches better if we did not use a representation based purely on cone contrasts. The cone contrast representation does not include any color appearance contribution from the background, and thus corresponds to a complete discounting of the background (e.g. Walraven, 1976; Werner & Walraven, 1981). This is a good basic assumption, but there are several reports in the literature in which the background is not discounted completely (e.g. Shevell, 1978; Chichilnisky & Wandell, 1996).

This model adds three new parameters corresponding to an additive color appearance effect from the background. The pattern–color separable model investigated above is a special case of this model, where the additive contribution from the background is zero. For subject KHB, this model includes 21 $(3 \times 3 + 9 + 3)$ parameters

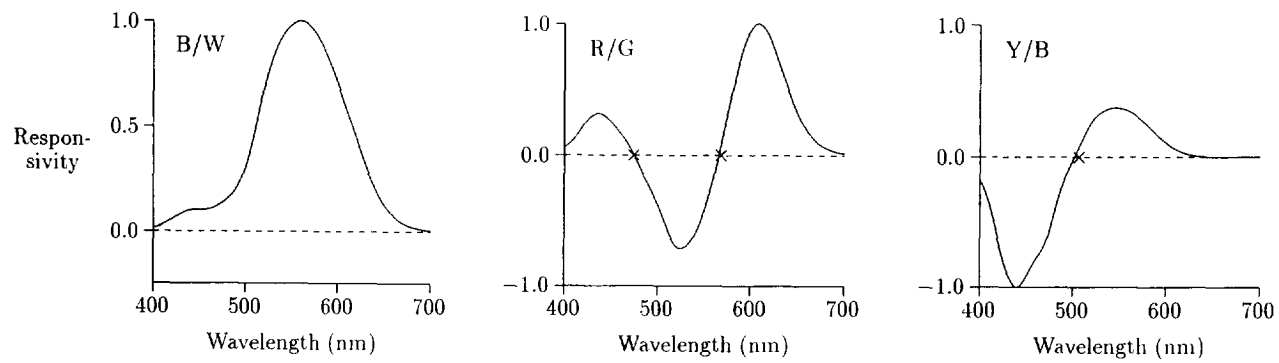

FIGURE 10. Color-responsivity function estimates. These estimates are based on fitting the pattern–color separable linear model to the whole data set of subject KHB. The functions can be classified as a black/white mechanism (B/W), a red/green mechanism (R/G) and a yellow/blue mechanism (Y/B). Estimates of the subject's unique blue, unique yellow and unique green, based on previous measurements of the subject's unique lines, are indicated by the ×. See text for details.

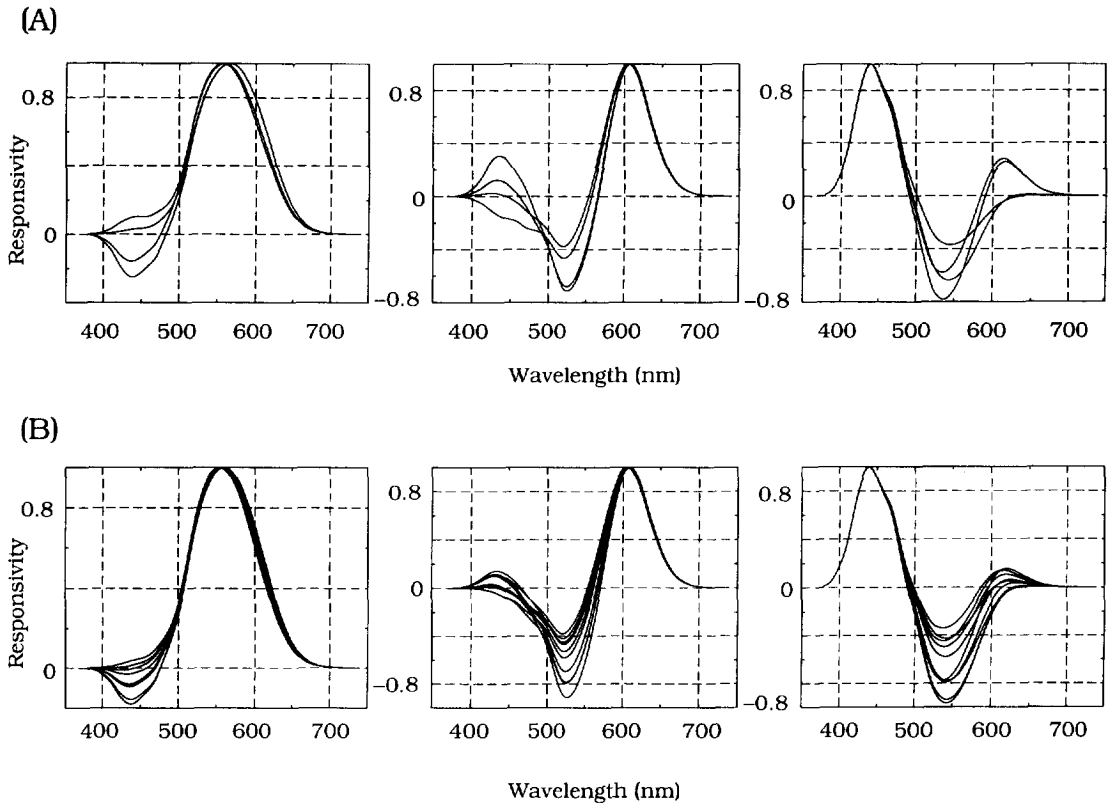

FIGURE 11. Comparison of color responsivity functions of four subjects and a set of simulated functions. (A) The estimated responsivity functions of two subjects from this study and two subjects from the study of Poirson and Wandell (1993). (B) The results perturbing the contributions of the L, M and S cones to each of the three wavelength responsivity functions are shown. The simulated curves were created by setting the mean cone contribution to each mechanism equal to the mean estimated from the data of the four observers. Then, Gaussian noise was added to each cone contribution and a new color-responsivity function was estimated. The variation in the simulated functions is similar to the variation in the estimated functions shown in (A).

to describe the 760 data points; for subject AF, it includes 18 ($2 \times 3 + 9 + 3$) parameters. Again, this general model does not substantially improve the fit to the data. For subject KHB, the residual error for this model was 3.33 compared to 3.57 for the more restrictive pattern–color separable model and, for subject AF, we found a residual error of 2.76 compared to 3.09 for the pattern–color separable model. Moreover, the cone coordinates of the effective background color fit by the model for subject KHB were (5.31, 5.07, 4.29); for subject AF, they were (5.45, 5.14, 5.15). Recall that the LMS coordinates of the uniform background were (5.32, 5.01, 4.49); see Method section.

DISCUSSION

Color-responsivity functions

As the measurements of color-matches to mixture gratings generally are consistent with pattern–color separability, it is reasonable to estimate the color and pattern-responsivity functions of the three putative mechanisms. Table 3 shows the color transformation matrices **C** estimated for our two subjects. The matrix rows define the relative contributions of the L, M and S cone photopigment absorptions to that mechanism.

Figure 10 is one graphical representation of the color-responsivity functions. The color responsivity of each color mechanism is plotted as a function of wavelength. These wavelength responsivity curves are calculated from the entries of the color transformation matrices as follows. The ith row contains the relative contributions of L, M and S cones for the ith mechanism. Hence, the spectral responsivity of the ith mechanism is:

$$c_{i1}L(\lambda) + c_{i2}M(\lambda) + c_{i3}S(\lambda)$$

where $L(\lambda)$, $M(\lambda)$ and $S(\lambda)$ are the spectral responsivities of L, M and S cones, respectively.

The three color-responsivity functions estimated from the data in this study are consistent with a general opponent-colors organization of color appearance. One function is spectrally broadband with a peak responsivity near 560 mn. The other two functions are spectrally opponent, similar to a red/green and a yellow/blue mechanism. These functions, estimated using isolated squarewaves and their mixtures, are similar to the ones estimated by Poirson and Wandell (1993) using only isolated squarewave test patterns.

Figure 11(A) shows the color-responsivity functions of two subjects from the Poirson and Wandell study together with the functions estimated in this study. Qualitatively, the color-responsivity functions from these two experi-

TABLE 4. Pattern-responsivity matrices $\mathbf{D}_f$ for the best-fitting pattern–color separable linear model*

Subject	Frequency	Pattern matrices $\mathbf{D}_f$ B/W	R/G	Y/B
AF	1 c/deg	0.978	0.900	0.764
	2 c/deg	0.969	0.887	0.618
KHB	1 c/deg	1.068	0.729	0.613
	2 c/deg	1.143	0.621	0.402
	4 c/deg	0.904	0.482	0.310

*The spatial scale factors associated with each color mechanism are shown in separate columns. B/W: black/white, R/G: red/green, Y/B: yellow/blue.

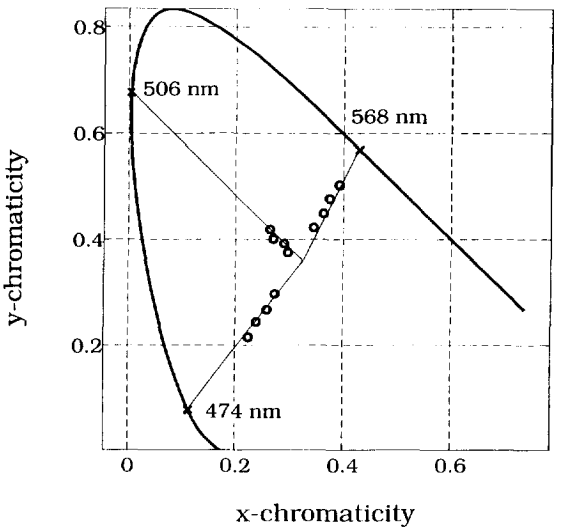

FIGURE 12. Unique hues. The CIE *xy*-chromaticity coordinates for unique blue, unique green and unique yellow measured at four different saturation levels on an isoluminant plane of 25 cd/m^2 are shown. The coordinates for each unique hue are fitted by straight lines. By extrapolating these lines to the spectrum locus, it is possible to estimate the unique hue wavelengths. The measurements stem from a previous study by one of us (Bäuml, 1993) (subject KHB).

ments have the same characteristics, though there is some obvious variation between the observers. For instance, the putative yellow/blue mechanism shows a zero-crossing at about 590 nm for two of the subjects, but no such zero-crossing for the other two subjects.

A portion of the variation between the observers is due to real differences in the contributions of the cone types to the different visual mechanisms, and another portion is due to experimental error. To investigate the effect of small variations in the real contributions of the L, M and S cones on the wavelength-responsivity functions, we performed the following simulation. First, we estimated the mean color-responsivity function, averaged across the four observers, for each of the three mechanisms. Then, we added a normally distributed noise term to each of the weights. The noise had zero mean and SD = 0.1 for the cone contributions to the black/white and yellow/blue mechanisms, and SD = 0.05 for the contributions to the red/green mechanism. When we used these SDs for the simulation, the variation we observed in the simulation was similar to the variation we observed in the functions estimated from the four subjects. Figure 11(B) shows the results of sampling ten color-responsivity functions created by this random process. The variation that we observed in the simulation is similar to the variation we observed in the functions estimated from the four subjects.

Pattern-responsivity functions. Table 4 shows the pattern responsivity matrices $\mathbf{D}_f$ estimated for our two subjects. Since subject KHB made matches for patterns of 1, 2 and 4 c/deg, we could estimate coefficients for three spatial frequencies. For subject AF, who did matches for patterns of 1 and 2 c/deg, we could estimate coefficients for only two spatial frequencies.

The estimated coefficients suggest the putative black/white mechanism to be bandpass, and the two putative opponent mechanisms to be lowpass. This holds especially for subject KHB. The pattern responsivity for this subject parallels those from the two subjects of the Poirson and Wandell (1993) study. The pattern for subject AF is similar to these three subjects with respect to the putative black/white and yellow/blue mechanisms; however, it shows some deviation with respect to the putative red/green mechanism. This subject's red/green mechanism reveals no major effect of spatial pattern for frequencies of 1 and 2 c/deg.

Effects of spatial variables on the color appearance of test lights have already been found in previous studies (Middleton & Holmes, 1949; Ingling *et al.*, 1970; Elsner *et al.*, 1987). Our results and those of Poirson and Wandell (1993, 1996), however, extend these earlier studies in two ways. First, we measured the effects of pattern systematically using spatial patterns and their spatial mixtures in order to form a more complete understanding of the effects. Second, we provided a quantitative model, based on the principle of pattern–color separability, to account for our data. We plan to extend the model to other (non-periodic, multiple orientations) stimulus patterns in the future.

Unique hues

The color-responsivity functions we estimated from our subjects are based on an appearance judgment, but they are not based on judgments of color opponency, such as one measures in the hue cancellation experiment. To the extent that the color-responsivity functions we measured are related to the appearance of opponent-colors, we might expect the zero-crossings of the color responsivity mechanisms to correspond to the unique hues measured with the hue cancellation method.

The color-responsivity function of subject KHB's estimated red/green mechanism has two zero-crossings, one at wavelength 474 nm, and the other at wavelength 566 nm. These two zero-crossings should correspond to unique blue and unique yellow. The color-responsivity function of his estimated blue/yellow mechanism shows

one zero-crossing at wavelength 501 nm that should correspond to unique green. Bäuml (1993) reported measurements of the unique hues for subject KHB, and these can be compared with the zero-crossings of the mechanisms estimated in the present study. Bäuml's measurements were made using isoluminant (25 cd/m^2) test patterns at four different saturation levels, so that his viewing conditions were quite similar to the ones used in the experiments reported here. Figure 12 shows the estimated CIE 1931 *xy*-chromaticity coordinates of the hues. As a first-order approximation, we assume that Bezold-Brücke and Abney hue invariance hold (Westphal, 1909; Purdy, 1931; Boynton & Gordon, 1965; Larimer *et al.*, 1974, 1975; but see Burns *et al.*, 1984, because they do not think the extrapolations are all that straight). Thus, we can derive the unique hue wavelengths for this observer. Specifically, straight lines are fit through the (x,y) coordinates and these lines are extrapolated to the spectral locus of the chromaticity diagram. Using this method, unique blue is located at 474 nm, unique green is located at 506 nm and unique yellow is located at 568 nm. These three wavelengths are close to the zero-crossings of the two putative opponent mechanisms we derived from our data (see Fig. 12).

The pattern-asymmetric color-matching experiments do not presuppose the existence of opponent-mechanisms, nor do they require the subject to make opponent-colors judgments. Even so, the zero-crossings of the color-responsivity functions are very close to the unique hues measured in the hue cancellation paradigm, whose design presupposes color-opponency (Brückner, 1927; Jameson & Hurvich, 1951). The color-matching and hue cancellation paradigms both involve appearance judgements, so that the agreement between the zero-crossings and unique hues may arise because the two experiments measure the responsivity of common perceptual mechanisms. To test this hypothesis further, one might compare the covariation of the zero-crossings and unique hues under various states of adaptation and for various types of dichromatic observers.

Model limitations

The empirical properties of superposition and pattern–color separability are both necessary conditions to derive meaningful and general estimates of pattern and color responsivity. Hence, in the first round of measurements, encompassing this study as well as the two others by Poirson and Wandell (1993, 1996), we have set a high threshold for rejecting linearity or separability. It remains our view that these properties hold well enough so that color- and pattern-responsivity function estimates made by assuming these empirical properties are useful to explain most of our results and to use as a basis for generalization to other similar experimental conditions. We regard the difference between the precision of the subjects' replications of their matches and the model predictions small enough to make the model useful for many types of engineering applications.

By accepting these properties in our analyses, however, we do not mean to imply that linearity and separability are precisely true, nor that they hold over an enormous range of viewing conditions. Many simple statistical tests can reject the null hypotheses of linearity and separability, particularly if we focus on portions of the data. Up to now, such deviations from linearity and separability have been treated as a nuisance so that we might interpret the basic behavioral results. In the future, these deviations may serve as clues about how to improve the predictions of these models and expand their empirical domain. In this section, we comment on some of the deviations that we have observed and some ways we believe our models should be extended.

The most consistent deviation from linearity we have seen is shown in Fig. 7. These data are from matches using mixture gratings consisting of a 2 or 4 c/deg squarewave of fixed cone contrast superimposed on a 1 c/deg squarewave of varying cone contrast. Most of the matches to the grating's bars fall on two parallel lines, but from closer inspection of the figure it should be apparent that the lines are not strictly parallel: the line corresponding to the isolated squarewave usually has a somewhat steeper slope than the lines corresponding to the mixture of the gratings. This deviation is reliable under the conditions shown in Fig. 7.

Second, the S cone data for the mixture grating in Fig. 6, for example, are not odd symmetric through the origin (see also Poirson & Wandell, 1993). Were a straight line fit separately through the data of the first and the third quadrants, the data in each quadrant would be linear, but the two line segments would be bent at the origin of the coordinate system. These deviations are neither numerous nor strong in our data, which probably explains why our attempts to fit the complete set of data using a model with increment/decrement asymmetries did not substantially improve the results. Perhaps by focusing on conditions in which these asymmetries are strong, we could learn more.

Third, we found failures of pattern-superposition in cases where the matching contrasts to the mixture gratings' bars were weak (see the S cone data of Fig. 7). Failures of linearity for low contrast patterns should be expected because Georgeson and Sullivan (1978) and Poirson and Wandell (1993) have shown already that simple linearity tests fail for low contrast gratings. Indeed, measurements of color appearance near threshold seem to provide a fundamental problem for linear theories in many experimental situations (Whittle & Challands, 1969; Walraven, 1976; Shevell, 1978). A substantial fraction of our measurements were made using low contrast targets, so that a substantial fraction of the model deviations probably are due to errors in predicting low contrast matches.

Model extensions

In describing and analyzing the color-matches, we used a stimulus-based representation. This simplifies our analysis and description of the behavior, and it also permits us to summarize the measurements in a manner

that can be applied directly to engineering applications of our work. There are various ways to extend our analysis, however, in order to clarify the neurophysiological basis of the results.

First, by taking into account the chromatic aberration of the eye, we will obtain a better estimate of the true cone contrasts. We decided to begin by developing an approximation to the matches that will be satisfactory for use in practical applications; in these applications, stimulus measurements must be made from the display screen, not from the retinal image. Much can be learned from extending our approach and eliminating chromatic aberration or correcting for it (see e.g. Mullen, 1985; Sekiguchi *et al.*, 1993; Marimont & Wandell, 1994).

Second, the experiments and analysis are framed as if the subjects set matches between the stimulus, as measured at the center of the bars, and the center of the uniform box. The stimulus contrast at the pattern edges is not considered. Given the importance of edges, this assumption seems unlikely.

A more complete process model, i.e. a model in which we render a full calculation based on a theoretical neural image, should help us understand the role of pattern in specifying the key locations within the image that determine color appearance.

SUMMARY

We measured the color appearance of bars within squarewave mixture gratings and evaluated whether the color appearance of these bars can be predicted from the color appearance of the bars in the squarewave components. We found that the asymmetric color-matches approximately satisfied contrast-homogeneity and pattern-superposition, making it possible to predict the color appearance of mixtures from the color appearance of the components.

Next we evaluated a series of model fits to the matches. A pattern–color separable linear model predicted the data about as well as any of the other more general models we examined. The pattern–color separable model predicted the matches with an error that was about twice as large as the variability of repeated matches.

The pattern–color separable model is associated with three theoretical mechanisms that have well-defined color and pattern responsivities. Because the model fits the data reasonably well, we explored the properties of these three mechanisms. We found that the pattern–color separable mechanisms we infer from these color-matches have an opponent-colors structure. The all-positive mechanism has a bandpass pattern-responsivity function and the two chromatic mechanisms have lowpass pattern-responsivity functions.

The pattern–color separable model provides a good first-order approximation to these low spatial frequency targets and their mixtures, although certain aspects of the data are not perfectly described by the model. Specifically, the model performs less well near threshold and there are certain reliable deviations when measuring the mixtures of simple patterns.

The consistency of the mechanism estimates across experiments and experimental conditions, ranging from matches to individual gratings, mixtures of gratings and unique hue settings, suggests that the first-order approximation by a pattern–color separable linear model describes an important part of the basic system architecture related to color appearance of low frequency colored patterns.

REFERENCES

Bäuml, K.-H. (1993). A ratio principle for a red/green and a yellow/blue channel? *Perception & Psychophysics, 53*, 338–344.

Bäuml, K.-H. (1994). Color appearance: Effect of illuminant changes under different surface collections. *Journal of the Optical Society of America A, 11*, 531–543.

Bäuml, K.-H. (1995). Illuminant changes under different surface collections: Examining some principles of color appearance. *Journal of the Optical Society of America A, 12*, 261–271.

Bowen, R. W., Pokorny, J. L. & Smith, V. C. (1989). Sawtooth contrast sensitivity: Decrements have the edge. *Vision Research, 29*, 1501–1509.

Boynton, R. M. & Gordon, J. (1965). Bezold–Brücke hue shift measured by color-naming technique. *Journal of the Optical Society of America, 55*, 78–86.

Brainard, D.H. (1989). Calibration of a computer controlled color monitor. *Color Research and its Applications, 14*, 23–34.

Brainard, D. H. & Wandell, B. A. (1992). Asymmetric color matching: how the illuminant affects color appearance. *Journal of the Optical Society of America A, 9*, 1433–1488.

Brückner, A. (1927). Zur Frage der Eichung von Farbsystemen. *Zeitschrift für Sinnesphysiologie, 58*, 322–362.

Burns, S. A., Elsner, A. E., Pokorny, J. & Smith, V. (1984). The Abney-effect: Chromaticity coordinates of unique and other constant hues. *Vision Research, 24*, 479–489.

Chichilnisky, E.-J. & Wandell, B. A. (1995). Photoreceptor sensitivity changes explain color appearance shifts induced by large uniform backgrounds in dichoptic matching. *Vision Research, 35*, 239–254.

Chichilnisky, E.-J. & Wandell, B. A. (1996). Seeing gray through the ON- and OFF-pathways. *Visual Neuroscience, 13*, 591–596.

du Buf, J. M. H. (1992). Brightness versus apparent contrast: I. Incremental and decremental disks with varying diameter. *Spatial Vision, 6*, 159–182.

Elsner, A. E., Burns, S. A. & Pokorny, J. (1987). Changes in constant-hue loci with spatial frequency. *Color Research and its Applications, 12*, 42–50.

Fairchild, M. D. & Berns, R. S. (1993). Image color-appearance specification through extension of CIELAB. *Color Research and its Applications, 18*, 178–190.

Fairchild, M. D. & Lennie, P. (1992). Chromatic adaptation to natural and incandescent illuminants. *Vision Research, 32*, 2077–2085.

Georgeson, M. A. & Sullivan, G. D. (1978). Contrast constancy: Deblurring in human vision by spatial frequency channels. *Journal of Physiologie, 253*, 627–656.

Ingling, C. R. Jr, Scheibner, H. M. O. & Boynton, R. M. (1970). Color naming of small foveal fields. *Vision Research, 10*, 501–511.

Jameson, D. & Hurvich, L. M. (1951). Use of spectral hue-invariant loci for the specification of white stimuli. *Journal of Experimental Psychology, 41*, 455–463.

Krauskopf, J. (1980). Discrimination and detection of changes in luminance. *Vision Research, 20*, 671–677.

Larimer, J., Krantz, D. H. & Cicerone, C. C. (1974). Opponent process additivity — I. Red/green equilibria. *Vision Research, 14*, 1127–1140.

Larimer, J., Krantz, D. H. & Cicerone, C. C. (1975). Opponent process additivity — II. Yellow/blue equilibria and nonlinear models. *Vision Research, 15*, 723–731.

Marimont, D. H. & Wandell, B. A. (1994). Matching color images: The effects of axial chromatic aberration. *Journal of the Optical Society of America A, 11*, 3113–3122.

Mausfeld, R. & Niederee, R. (1993). An inquiry into the relational concepts of colour, based on incremental principles of colour coding for minimal relational stimuli. *Perception, 22*, 427–462.

Middleton, W. E. K. & Holmes, M. C. (1949). The apparent colors of surfaces of small subtense — a preliminary report. *Journal of the Optical Society of America, 39*, 582–592.

Mullen, K. (1985). The contrast sensitivity of human colour vision to red–green and blue–yellow chromatic gratings. *Journal of Physiology, 359*, 381–400.

Poirson, A. B. & Wandell, B. A. (1993). The appearance of colored patterns: Pattern–color separability. *Journal of the Optical Society of America A, 10*, 2458–2470.

Poirson, A. B. & Wandell, B. A. (1996). Detection of colored patterns: pattern–color separability. *Vision Research 36*, 515–526.

Purdy, D. M. (1931). Spectral hue as a function of intensity. *American Journal of Psychology, 49*, 313–315.

Schiller, P. H., Sandell, J. H. & Maunsell, J. H. R. (1986). Functions of the ON and OFF channels of the visual system. *Nature, 322*, 824–825.

Sekiguchi, N., Williams, D. R. & Brainard, D. H. (1993). Aberration-free measurements of the visibility of isoluminant ratings. *Journal of the Optical Society of America A, 10*, 2105–2117.

Shevell, S. K. (1978). The dual role of chromatic backgrounds in color perception. *Vision Research, 18*, 1649–1661.

Smith, V. & Pokorny, J. (1975). Spectral sensitivity of the foveal cone photopigments between 400 and 700 nm. *Vision Research, 15*, 161–171.

Walraven, J. (1976). Discounting the background — the missing link in the explanation of chromatic adaptation. *Vision Research, 16*, 289–295.

Walraven, J. (1977). Colour signals from incremental and decremental light stimuli. *Vision Research, 17*, 71–76.

Wandell, B. A. (1993). Color appearance: The effects of illumination and spatial pattern. *Proceedings of the National Academy of Science, 90*, 9778–9784.

Wandell, B. A. (1995). *Foundations of vision*. Sunderland, MA: Sinauer.

Werner, J. & Walraven, J. (1981). Effect of chromatic adaptation on the achromatic locus: The role of contrast, luminance and background color. *Vision Research, 22*, 929–943.

Westphal, H. (1909). Unmittelbare Bestimmung der Urfarben. *Zeitschrift für Sinnesphysiologie, 44*, 182–230.

White, T. W., Irvin, G. E. & Williams, M. C. (1980). Asymmetry in the brightness and darkness Broca–Sulzer effects. *Vision Research, 20*, 723–726.

Whittle, P. (1986). Increments and decrements: Luminance discrimination. *Vision Research, 26*, 1677–1692.

Whittle, P. & Challands, P. D. C. (1969). The effect of background luminance on the brightness of flashes. *Vision Research, 9*, 1095–1109.

Acknowledgements—We thank the referees for their comments on an earlier version of the paper. Karl-Heinz Bäuml received support from Deutscher Akademischer Austauschdienst and Brian Wandell was supported in part by NEI RO1 EY03164 and NASA 2-307.